
INCREMENTAL ADAPTIVE DYNAMIC PROGRAMMING FOR APPROXIMATE OPTIMAL TRACKING CONTROL: A DECOUPLED AND MODEL-FREE APPROACH

THIS WORK HAS BEEN SUBMITTED TO THE IEEE FOR POSSIBLE PUBLICATION. COPYRIGHT MAY BE TRANSFERRED WITHOUT NOTICE, AFTER WHICH THIS VERSION MAY NO LONGER BE ACCESSIBLE.

Cong Li
cong.li@tum.de

Yongchao Wang
yongchao.wang@tum.de

Fangzhou Liu*
fangzhou.liu@tum.de

Martin Buss
mb@tum.de

ABSTRACT

This paper proposes a new formulation for the optimal tracking control problem (OTCP) of Euler-Lagrange systems. This formulation extends the incremental adaptive dynamic programming (IADP) technique, a reinforcement learning based method for solving the robust optimal regulation control problem (RORCP), to learn the approximate solution to the OTCP. Departing from available solutions to the OTCP, our developed tracking control scheme settles the curse of complexity problem in value function approximation from a decoupled way, circumvents the learning inefficiency regarding varying desired trajectories by avoiding introducing a reference trajectory dynamics into the learning process, and requires neither an accurate nor identified dynamics through the time delay estimation technique. Specifically, we first convert the intractable OTCP of a high-dimensional uncertain system into multiple manageable sub-RORCPs of low-dimensional incremental error subsystems. Then, the resulting sub-RORCPs are approximately solved by IADP implemented as a parallel critic learning structure. The proposed tracking control scheme is developed with rigorous theoretical analysis of system stability and weight convergence, and validated numerically on a 6-DoF quadrotor and experimentally on a 3-DoF robot manipulator.

Keywords Optimal tracking control · incremental adaptive dynamic programming · reinforcement learning · decoupled control · time delay estimation

1 Introduction

The optimal tracking control problem (OTCP) has been the focus of the control community, where both tracking error deviations and control energy expenditures serve as performance indexes to be optimized (see [1, 2], and the references therein). To address the OTCP, recently adaptive dynamic programming (ADP), which is a reinforcement learning (RL) based control approach, emerges as an efficient method to approximately solve the algebraic Riccati equation (ARE) or Hamilton Jacobi Bellman (HJB) equation forwardly via an actor-critic or a critic-only neural network (NN) learning structure [3]. Although RL-based ADP tackles the curse of dimensionality problem, and enjoys promising performance as well as desired theoretical guarantees (e.g., rigorous proofs of system stability and weight convergence), several bottlenecks remain to be investigated for ADP's practical implementation on the OTCP: a) value function approximation for a high-dimensional system; b) efficient learning regarding varying desired trajectories; and c) low-cost model-free control strategies. In particular, the number of activation functions required for an accurate value function approximation grows exponentially with the system dimension [4]. The existing ADP based OTCP solutions [5, 6, 7], trained on augmented systems (composed of an assumed reference trajectory dynamics and a controlled plant dynamics), are sensitive to reference trajectory dynamics. This is because multiple different desired trajectories would lead to varying augmented systems. Thereby, the associated training process repeatedly restarts but might without satisfying tracking performance in each learning period. To achieve model-free control, either parametric [8, 9, 10] or non-parametric methods [11, 12, 13] result in nontrivial computational loads and/or complexity that are unfavourable to practical applications. This paper aims to address the bottlenecks mentioned above via our developed tracking control scheme.

1.1 Related works

The common OTCP introduces a value function that includes quadratic terms about tracking errors and control inputs [1, 2]. The persistently exciting tracking control inputs result in time-varying (unbounded) value functions that NNs cannot directly approximate as the NN approximation scheme can only approximate functions within a compact set [14, 15]. To address this technical obstacle, mainly two approaches are proposed to transform the time-varying value function into a time-invariant counterpart that NNs could approximate. The first approach uses a vanishing feedback control input associated input penalty function, rather than a non-vanishing total control input (i.e., a sum of feed-forward and feedback control terms) related one, to facilitate a time-invariant value function [5, 6]. From a different perspective, the second approach uses a discount factor to suppress the originally unbounded value function [7]. The aforementioned solutions [5, 6, 7] to the OTCP formulate on an assumed reference trajectory dynamics. Although effective, these approaches suffer the flexibility problem [16]. In particular, the tracking control strategy trained on one specific reference trajectory dynamics cannot efficiently track the unaccounted reference signals. Even though a new reference trajectory dynamics is available to characterize the changed desired trajectory, the tracking control strategy has to be retrained on a new associated augmented system for a specific period before getting a satisfying tracking performance. This is unfavourable to practical realtime applications. For example, in a dynamic environment populated with moving obstacles, a quadrotor keeps on replanning to generate safe desired trajectories, which are accounted for by multiple reference trajectory dynamics. Thereby, the controller training processes in the works above [5, 6, 7] restart as replanning happens. However, the tracking performance during each limited training period is usually not satisfying for practical applications, especially considering safety issues demanding of perfect tracking precision.

Except for the flexibility problem mentioned above, the scalability of ADP based optimal tracking control strategy to high-dimensional systems remains to be investigated. The obstacle lies in the so-called curse of complexity. Specifically, the required number of activation functions to gain a sufficiently accurate approximation of a value function grows exponentially with the system dimension. The existing approaches to the OTCP [5, 6, 7] further worsen this complexity problem because the utilized augmented system doubles the original system dimension and thus slows down the value function learning process. Theoretically, practitioners could seek a sufficient large NN to achieve a satisfying approximation of a high-dimensional value function [14]. However, practically, this is nontrivial considering that appropriate activation functions are usually chosen by trial and error. This process is tedious and time-consuming. Even though a suitable set of activation functions and appropriate hyperparameters are found through engineering efforts, the accompanying computation load jeopardises the realtime performance of the associated weight update law and control strategy [8]. Thus, experimental validations of ADP based optimal tracking control strategy on a high-dimensional system is seldom found in existing works. Few ADP related works aim to solve this bottleneck scalability problem except [4], where the state following (StaF) kernel method is developed to decrease the number of activation functions needed for the value function approximation. However, the desired NN weight convergence, which is favorable to improve robustness and performance, is lost [4]. It is worth mentioning works that attempt to solve the high-dimensional value function approximation problem by using the powerful approximation ability of deep neural networks (DNNs) [17]. Although promising, DNN related methods lack a rigorous mathematical analysis.

Another critical issue not fully considered in existing ADP based solutions to the OTCP is a low-cost model-free tracking control strategy for practical applications. The desired model-free control strategy could be accomplished by identifying dynamics explicitly through NNs [8, 9], fuzzy logic systems [11], Gaussian process [12], or observer [13]. Unlike these computation-intensive approaches, the time delay estimation (TDE) technique [18, 19] emerges as an easy-to-implement alternative to achieve model-free control by reusing measured past input-state signals.

1.2 Contribution

This work develops an IADP based tracking control scheme to address the flexibility, scalability, and model-free issues mentioned above. The contributions are summarized as follows.

- A new formulation for the OTCP of Euler-Lagrange (E-L) systems is proposed to avoid using an assumed reference trajectory dynamics in the learning process. Thereby, the flexibility of the tracking control scheme is extended.
- A high-dimensional system's intractable value function approximation problem is conquered by dividing it into multiple low-dimensional subsystem's value function approximation problems. The decoupled control technique endows our proposed tracking control scheme with scalability to systems in arbitrary dimensions.
- The time-delayed signals are reused to facilitate a model-free tracking control strategy, which estimate the unknown model knowledge and the decoupled control related coupling terms without conducting laborious system identification processes.

The organization of this paper is as follows. Section 2 first presents the OTCP formulation. Then, the development of incremental subsystems is shown in Section 3. Thereafter, Section 4 presents the proposed tracking control scheme. Moreover, Section 5 elucidates the approximate solution to the OTCP. The developed tracking control scheme is numerically and experimentally validated in Section 6 and Section 7, respectively. Finally, the conclusion is drawn in Section 8.

Notations: Throughout this paper, \mathbb{R} denotes the set of real numbers; \mathbb{R}^n is the Euclidean space of n -dimensional real vector; $\mathbb{R}^{n \times m}$ is the Euclidean space of $n \times m$ real matrices; $\|\cdot\|$ represents the Euclidean norm for vectors and induced norm for matrices; x_i (E_{ij}) is the i -th (ij -th) entry of a vector $x \in \mathbb{R}^n$ (matrix $E \in \mathbb{R}^{n \times m}$); $\text{diag}(x)$ is the $n \times n$ diagonal matrix with the i -th diagonal entry equals x_i . For notational brevity, time-dependence is suppressed without causing ambiguity.

2 Problem formulation

Considering the following E-L equation :

$$M(q)\ddot{q} + N(q, \dot{q}) + F(\dot{q}) = \tau, \quad (1)$$

where $M(q) : \mathbb{R}^n \rightarrow \mathbb{R}^{n \times n}$ is the symmetric positive definite inertia matrix; $N(q, \dot{q}) = C(q, \dot{q})\dot{q} + G(q) : \mathbb{R}^n \times \mathbb{R}^n \rightarrow \mathbb{R}^n$, $C(q, \dot{q}) : \mathbb{R}^n \times \mathbb{R}^n \rightarrow \mathbb{R}^{n \times n}$ is the matrix of centrifugal and Coriolis terms, $G(q) : \mathbb{R}^n \rightarrow \mathbb{R}^n$ represents the gravitational terms; $F(\dot{q}) : \mathbb{R}^n \rightarrow \mathbb{R}^n$ denotes the viscous friction; $q, \dot{q}, \ddot{q} \in \mathbb{R}^n$ are the vectors of angles, velocities, and accelerations, respectively; $\tau \in \mathbb{R}^n$ represents the input torque vector. Assume that $M(q)$, $C(q, \dot{q})$, $G(q)$, and $F(\dot{q})$ are unknown. Note that the mathematical model (1) is provided here for later theoretical analysis. Our developed tracking control scheme requires no explicit model knowledge.

The control objective is to design a model-free tracking control strategy τ to enable the plant (1) to track a prior-given desired trajectory $x_d = [q_d^\top, \dot{q}_d^\top]^\top \in \mathbb{R}^{2n}$ while minimizing a predefined performance function. The OTCP mentioned above is nontrivial given the high-dimensional and highly uncertain dynamics (1). The following sections clarify our proposed tracking control scheme to address the considered OTCP.

3 Incremental subsystem

This section benefits from the decoupled control and TDE techniques [20, 21] to develop incremental subsystems. The formulated incremental subsystems are equivalent to the dynamics (1), but no explicit model information is required. Specifically, the decoupled control technique is first utilized to divide the high-dimensional system into multiple low-dimensional subsystems. Then, the TDE technique is introduced to address the unknown dynamics as well as the decoupled control related coupling terms. Here the constructed incremental subsystems serve as basis to design the model-free tracking control strategy in Section 4, and allow us to address the scalability problem of the value function approximation in Section 5.1.

The high-dimensional system (1) can be decoupled into multiple subsystems, wherein the i -th subsystem follows

$$M_{ii}\ddot{q}_i + H_i = \tau_i, \quad i = 1, 2, \dots, n, \quad (2)$$

where $H_i = \sum_{j=1, j \neq i}^n M_{ij}\ddot{q}_j + N_i + F_i \in \mathbb{R}$ is a lumped term that embodies the coupling terms (i.e., $\sum_{j=1, j \neq i}^n M_{ij}\ddot{q}_j$) and the unknown model knowledge (i.e., N_i, F_i). Note that H_i could be generalized to represent unmodeled dynamics and/or potential external disturbances.

For convenience, by denoting $x_i = [x_{i1}, x_{i2}]^\top = [q_i, \dot{q}_i]^\top \in \mathbb{R}^2$, and $u_i = \tau_i \in \mathbb{R}$, we rewrite (2) as

$$\dot{x}_{i1} = x_{i2}, \quad (3a)$$

$$\dot{x}_{i2} = f_i(x_i) + g_i(x_i)u_i, \quad (3b)$$

where $f_i(x_i) = -H_i/M_{ii} \in \mathbb{R}$, and $g_i(x_i) = 1/M_{ii} \in \mathbb{R}$ are unknown. These unknown functions hinder us to directly design tracking controllers based on the subsystem (3). Departing from common methods that identify the unknown $f_i(x_i)$, $g_i(x_i)$ explicitly through a tedious identification process [8, 9, 10, 11, 12, 13], we exploit time-delayed signals to estimate the unknown model knowledge.

To achieve time delay estimation, we first introduce a predetermined constant $\bar{g}_i \in \mathbb{R}^+$ and multiply \bar{g}_i^{-1} on (3b),

$$\bar{g}_i^{-1}\dot{x}_{i2} = h_i(x_i, \dot{x}_{i2}) + u_i(x_i), \quad (4)$$

where $h_i(x_i, \dot{x}_{i2}) = (\bar{g}_i^{-1} - g_i^{-1}(x_i))\dot{x}_{i2} + g_i^{-1}(x_i)f_i(x_i) \in \mathbb{R}$ is a lumped term that embodies the unknown model knowledge $f_i(x_i)$, $g_i(x_i)$ of (3b).

Then, with a sufficiently high sampling rate¹ [18, 19], by utilising the TDE technique, the unknown $h_i(x_i, \dot{x}_{i2})$ in (4) could be estimated by time-delayed signals as

$$\hat{h}_i(x_i, \dot{x}_{i2}) = h_{i,0}(x_{i,0}, \dot{x}_{i2,0}) = \bar{g}_i^{-1} \dot{x}_{i2,0} - u_{i,0}, \quad (5)$$

where $u_{i,0} = u_i(t-L)$, $\dot{x}_{i2,0} = \dot{x}_{i2}(t-L)$. The delay time $L \in \mathbb{R}^+$ is directly chosen as the sampling period, which is the smallest achievable value of L in practical implementations, to achieve an accurate estimation of $h_i(x_i, \dot{x}_{i2})$ [19].

By substituting (5) into (4), we get

$$\dot{x}_{i2} = \dot{x}_{i2,0} + \bar{g}_i(\Delta u_i + \xi_i), \quad (6)$$

where $\Delta u_i = u_i - u_{i,0} \in \mathbb{R}$ is the incremental control input; $\xi_i = h_i(x_i, \dot{x}_{i2}) - \hat{h}_i(x_i, \dot{x}_{i2}) \in \mathbb{R}$ denotes the so-called TDE error that is proved to be bounded in Section 4 Lemma 1.

Combining (3) with (6), we finally obtain the dynamics of the i -th incremental subsystem

$$\dot{x}_{i1} = x_{i2}, \quad (7a)$$

$$\dot{x}_{i2} = \dot{x}_{i2,0} + \bar{g}_i(\Delta u_i + \xi_i), \quad (7b)$$

which is an equivalent of (3) but without using explicit model information. This section has decoupled the original n -D (1) into n equivalent 2-D incremental subsystems (7). Accordingly, we transform the OTCP of (1) into n sub-OTCPs regarding (7). The following section will present our developed tracking control scheme by focusing on the sub-OTCP of (7).

Remark 1. *The decoupled control technique facilitates realtime control for a high-dimensional system by distributing the computation load into multiple processors. However, the utilized decoupled control technique presents a challenge of getting the value of the coupling terms, which is usually addressed by add-on tools such as (RBF) NNs [22, 23] that accompany with additional parameter tuning efforts and computational loads. Unlike these works, the TDE technique, which is introduced initially to achieve model-free control in a low-cost and easily implemented way (only a constant \bar{g}_i to be debugged), enjoys an additional benefit that compensates the coupling terms in (2). Furthermore, departing from the (deep) RL based model-free control method [24], utilizing TDE to achieve model-free control provides a mathematical form of incremental subsystem dynamics (7) that permits us to exploit the rich analysis tool from the control field to analyse the properties of our designed tracking controller, and provide theoretical guarantees.*

4 Tracking control scheme

This section details our proposed tracking control scheme, as displayed in Fig.1, to solve the sub-OTCP of (7). The incremental control input to be designed follows

$$\Delta u_i = \Delta u_{i_f} + \Delta u_{i_b}, \quad (8)$$

where the incremental dynamic inversion based $\Delta u_{i_f} \in \mathbb{R}$ serves to transform the time-varying sub-OTCPs into equivalent time-invariant sub-RORCPs in Section 4.1; and $\Delta u_{i_b} \in \mathbb{R}$ is an IADP based incremental control policy to optimally drive the tracking error to zero in Section 4.2. The detailed procedures to design Δu_{i_f} and Δu_{i_b} are clarified in Section 4.1 and Section 4.2, respectively.

4.1 Generation of incremental error subsystem

This subsection formulates the i -th incremental error subsystem via the properly chosen Δu_{i_f} . The formulated incremental error subsystem converts the sub-OTCP regarding (7) into its sub-RORCP, and facilitates the development of the optimal incremental control policy in Section 4.2. The detailed procedures to design Δu_{i_f} and to generate the incremental error subsystem are as follows.

Define $e_i = [e_{i1}, e_{i2}]^\top \in \mathbb{R}^2$, where $e_{i1} = x_{i1} - q_{d1} \in \mathbb{R}$ and $e_{i2} = x_{i2} - \dot{q}_{d1} \in \mathbb{R}$. Combining with (7b) and (8) yields

$$\dot{e}_{i2} = \dot{x}_{i2,0} + \bar{g}_i(\Delta u_{i_f} + \Delta u_{i_b} + \xi_i) - \ddot{x}_{r_i}. \quad (9)$$

By designing the required Δu_{i_f} in (9) as

$$\Delta u_{i_f} = \bar{g}_i^{-1}(\ddot{x}_{r_i} - \dot{x}_{i2,0} - k_{i1}e_{i1} - k_{i2}e_{i2}), \quad (10)$$

¹The so-called sufficiently high sampling rate, which is a prerequisite for estimating the unknown $h_i(x_i, \dot{x}_{i2})$ by reusing past measurements of states and control inputs, can be chosen as the value that is larger than 30 times the system bandwidth.

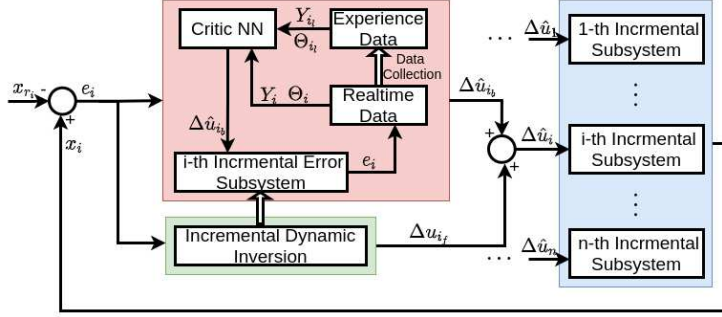


Figure 1: Schematic of the tracking control scheme. The blue area decouples the original OTCP into sub-OTCPs of incremental subsystems, as illustrated in Section 3; The green area converts the sub-OTCPs into equivalent sub-RORCPs of incremental error subsystems, as clarified in Section 4.1; The read area illustrates the solution to the transformed sub-RORCPs via IADP, as described in Section 4.2 and Section 5.

and substituting (10) into (9), we get

$$\dot{e}_{i_2} = -k_{i_1}e_{i_1} - k_{i_2}e_{i_2} + \bar{g}_i\Delta u_{i_b} + \bar{g}_i\xi_i, \quad (11)$$

where $k_{i_1}, k_{i_2} \in \mathbb{R}^+$ are parameters to be tuned.

Recall that $\dot{e}_{i_1} = e_{i_2}$. Then, combining with (11), we obtain the i -th incremental error subsystem

$$\dot{e}_i = A_i e_i + B_i \Delta u_{i_b} + B_i \xi_i, \quad (12)$$

where $A_i = \begin{bmatrix} 0 & 1 \\ -k_{i_1} & -k_{i_2} \end{bmatrix} \in \mathbb{R}^{2 \times 2}$, and $B_i = \begin{bmatrix} 0 \\ \bar{g}_i \end{bmatrix} \in \mathbb{R}^2$. The sub-OTCP of (7) illustrated in Section 3 is to optimally drive the values of e_i to zero. This is equivalent to the sub-RORCP of the incremental error subsystem (12) given the unknown ξ_i . In other words, by designing Δu_{i_f} in the form of (10), this subsection transforms the sub-OTCP of (7) into the sub-RORCP regarding (12).

Remark 2. The developed Δu_{i_f} (10) here acts as a supplementary control input to the Δu_{i_b} designed in Section 4.2. In particular, the utilized Δu_{i_f} generates an incremental error subsystem (12). Then, we train Δu_{i_b} on the formulated incremental error subsystem in Section 4.2. This practice departs from most of existing ADP related works for the OTCP [5, 6, 7], wherein the tracking control strategies are trained on one specific reference trajectory dynamics. Thus, the flexibility of our developed tracking control scheme against varying desired trajectories is improved without directly using reference signals in the learning process.

4.2 IADP for optimal incremental control policy

This subsection develops an optimal incremental control policy to solve the sub-RORCP of (12), i.e., robustly stabilizing the tracking error to zero in an optimal manner. Furthermore, we incorporate the TDE error ξ_i of (12) into the value function to deal with it under an optimization framework.

Given ξ_i in (12) is unknown, thus the available incremental error subsystem for later analysis follows

$$\dot{e}_i = A_i e_i + B_i \Delta u_{i_b}. \quad (13)$$

To stabilize (13) in an optimal manner, the value function is considered as

$$V_i(t) = \int_t^\infty r_i(e_i(\nu), \Delta u_{i_b}(\nu)) d\nu, \quad (14)$$

where $r_i(e_i, \Delta u_{i_b}) = e_i^\top Q_i e_i + W_i(\Delta u_{i_b}) + \bar{\xi}_{oi}^2$. The quadratic term $e_i^\top Q_i e_i$, where $Q_i \in \mathbb{R}^{2 \times 2}$ is a positive definite matrix, is introduced to improve the tracking precision. The input penalty function $W_i(\Delta u_{i_b})$ follows

$$W_i(\Delta u_{i_b}) = 2 \int_0^{\Delta u_{i_b}} \beta \tanh^{-1}(\vartheta/\beta) d\vartheta, \quad (15)$$

which is utilized to punish and enforce the optimal incremental control input as $\|\Delta u_{i_b}\| \leq \beta \in \mathbb{R}^+$. The limited Δu_{i_b} is beneficial since a severe interruption might lead to an abrupt change of Δu_{i_b} , which might destabilize the learning

process introduced in Section 5. The TDE error related term follows $\bar{\xi}_{oi} = \bar{c}_i \|\Delta u_{ib}\|$, where $\bar{c}_i \in \mathbb{R}^+$ is chosen as illustrated in Theorem 1. The proof given in Theorem 1 illustrates the rationality of incorporating $\bar{\xi}_{oi}$ into the value function to address the TDE error during the optimization process.

For $\Delta u_{ib} \in \Psi$, where Ψ is the set of admissible incremental control policies [19, Definition 1], the associated optimal value function follows

$$V_i^* = \min_{\Delta u_{ib} \in \Psi} \int_t^\infty r_i(e_i(\nu), \Delta u_{ib}(\nu)) d\nu. \quad (16)$$

Define the Hamiltonian function as

$$H_i(e_i, \Delta u_{ib}, \nabla V_i) = r(e_i, \Delta u_{ib}) + \nabla V_i^T (A_i e_i + B_i \Delta u_{ib}), \quad (17)$$

where $\nabla(\cdot) := \partial(\cdot)/\partial e_i$. Then, V_i^* satisfies the HJB equation

$$0 = \min_{\Delta u_{ib} \in \Psi} [H_i(e_i, \Delta u_{ib}, \nabla V_i^*)]. \quad (18)$$

Assume that the minimum of (16) exists and is unique [19, 25]. By using the stationary optimality condition on the HJB equation (18), we gain an analytical-form optimal incremental control strategy as

$$\Delta u_{ib}^* = -\beta \tanh\left(\frac{1}{2\beta} B_i^\top \nabla V_i^*\right). \quad (19)$$

To obtain Δu_{ib}^* , we need to solve the HJB equation (18) to determine the value of ∇V_i^* , which is detailly clarified in Section 5. In the following part of this subsection, based on the TDE error bound given in Lemma 1, we prove in Theorem 1 that the optimal incremental control policy Δu_{ib}^* (19) regarding (13) is the solution to the sub-RORCP of (12).

Lemma 1. *Given a sufficiently high sampling rate, $\exists \bar{\xi}_i \in \mathbb{R}^+$, there holds $\|\xi_i\| \leq \bar{\xi}_i$.*

Proof. Combing (4) with (5), the TDE error for the i -th subsystem (7) follows

$$\begin{aligned} \xi_i &= h_i - \hat{h}_i = h_i - h_{i,0} \\ &= (\bar{g}_i^{-1} - g_i^{-1})\Delta \dot{x}_{i2} + (\bar{g}_{i,0}^{-1} - g_{i,0}^{-1})\dot{x}_{i2,0} + g^{-1}(f_i - f_{i,0}) + (g_i^{-1} - g_{i,0}^{-1})f_{i,0}, \end{aligned} \quad (20)$$

where $\Delta \dot{x}_{i2} = \dot{x}_{i2} - \dot{x}_{i2,0}$. Based on (3b), (7b) and (8), an equivalent form of $\Delta \dot{x}_{i2}$ follows

$$\begin{aligned} \Delta \dot{x}_{i2} &= f_i + g_i u_i - f_{i,0} - g_{i,0} u_{i,0} \\ &= g_i \Delta u_i + (g_i - g_{i,0})u_{i,0} + f_i - f_{i,0} \\ &= g_i(\Delta u_{if} + \Delta u_{ib}) + (g_i - g_{i,0})u_{i,0} + f_i - f_{i,0}. \end{aligned} \quad (21)$$

Substituting (21) into (20), we get

$$\xi_i = (g_i \bar{g}_i^{-1} - 1)\Delta u_{if} + (g_i \bar{g}_i^{-1} - 1)\Delta u_{ib} + \delta_{1i}, \quad (22)$$

where $\delta_{1i} = \bar{g}_i^{-1}(g_i - g_{i,0})u_0 + \bar{g}_i^{-1}(f_i - f_{i,0})$.

For simplicity, denoting $\mu_i = \ddot{x}_{r_i} - k_{i1}e_{i1} - k_{i2}e_{i2} \in \mathbb{R}$. According to (5) and (10), Δu_{if} in (22) follows

$$\begin{aligned} \Delta u_{if} &= \bar{g}_i^{-1}(\mu_i - \bar{g}_i h_{i,0} - \bar{g}_i u_{i,0}) \\ &= \bar{g}_i^{-1}\mu_i - (\bar{g}_i^{-1} - g_{i,0}^{-1})\dot{x}_{i2,0} - g_{i,0}^{-1}f_{i,0} - u_{i,0} \\ &= \bar{g}_i^{-1}\mu_i - (\bar{g}_i^{-1} - g_{i,0}^{-1})(f_{i,0} + g_{i,0}u_{i,0}) - g_{i,0}^{-1}f_{i,0} - u_{i,0} \\ &= \bar{g}_i^{-1}\mu_i - \bar{g}_i^{-1}(f_{i,0} + g_{i,0}u_{i,0}) \\ &= \bar{g}_i^{-1}(\mu_i - \mu_{i,0}) - \bar{g}_i^{-1}(\dot{x}_{i2,0} - \mu_{i,0}), \end{aligned} \quad (23)$$

where $\mu_{i,0} = \ddot{x}_{r_{i,0}} - k_{i1}e_{i1,0} - k_{i2}e_{i2,0}$. Besides, combining (7b) with (8), we get

$$\begin{aligned} \dot{x}_{i2} &= \dot{x}_{i2,0} + \bar{g}_i(\Delta u_{if} + \Delta u_{ib}) + \bar{g}_i \xi_i \\ &= \dot{x}_{i2,0} + \bar{g}_i \bar{g}_i^{-1}(\mu_i - \dot{x}_{i2,0}) + \bar{g}_i \Delta u_{ib} + \bar{g}_i \xi_i \\ &= \mu_i + \bar{g}_i \Delta u_{ib} + \bar{g}_i \xi_i. \end{aligned} \quad (24)$$

Based on the result shown in (24), we get

$$\xi_i = \bar{g}_i^{-1}(\dot{x}_{i2} - \mu_i - \bar{g}_i \Delta u_{ib}). \quad (25)$$

Accordingly, the following equation establishes

$$\xi_{i,0} = \bar{g}_i^{-1}(\dot{x}_{i2,0} - \mu_{i,0} - \bar{g}_i \Delta u_{i_b,0}). \quad (26)$$

Based on the result given in (26), (23) is rewritten as

$$\begin{aligned} \Delta u_{i_f} &= \bar{g}_i^{-1}(\mu_i - \mu_{i,0}) - \bar{g}_i^{-1}(\dot{x}_{i2,0} - \mu_{i,0} - \bar{g}_i \Delta u_{i_b,0}) - \Delta u_{i_b,0} \\ &= \bar{g}_i^{-1}(\mu_i - \mu_{i,0}) - \xi_{i,0} - \Delta u_{i_b,0}. \end{aligned} \quad (27)$$

Substituting (27) into (22) yields

$$\xi_i = (1 - g_i \bar{g}_i^{-1}) \xi_{i,0} + (1 - g_i \bar{g}_i^{-1}) \bar{g}_i^{-1}(\mu_{i,0} - \mu_i) + (1 - g_i \bar{g}_i^{-1})(\Delta u_{i_b,0} - \Delta u_{i_b}) + \delta_{1i}. \quad (28)$$

In discrete-time domain, (28) can be represented as

$$\xi_i(k) = (1 - g_i(k) \bar{g}_i^{-1}) \xi_i(k-1) + (1 - g_i(k) \bar{g}_i^{-1}) \Delta \tilde{u}_{i_b} + \delta_{1i} + \delta_{2i}, \quad (29)$$

where $\Delta \tilde{u}_{i_b} = \Delta u_{i_b}(k-1) - \Delta u_{i_b}(k)$, $\delta_{2i} = (1 - g_i(k) \bar{g}_i^{-1}) \bar{g}_i^{-1}(\mu_i(k-1) - \mu_i(k))$.

The constrained input $\|\Delta u_{i_b}(k)\| \leq \beta$ implies that the following equation holds

$$\|\Delta \tilde{u}_{i_b}\| \leq \|\Delta u_{i_b}(k-1)\| + \|\Delta u_{i_b}(k)\| \leq 2\beta. \quad (30)$$

We choose the value of \bar{g}_i to meet $\|1 - g_i(k) \bar{g}_i^{-1}\| \leq \iota_i < 1$, where $\iota_i \in \mathbb{R}^+$. Under a sufficiently high sampling rate, it is reasonable to assume that there exists $\bar{\delta}_{1i}, \bar{\delta}_{2i} \in \mathbb{R}^+$ such that $\|\delta_{1i}\| \leq \bar{\delta}_{1i}$, and $\|\delta_{2i}\| \leq \iota_i \bar{\delta}_{2i}$. Then, the following equations hold:

$$\begin{aligned} \|\xi_i(k)\| &\leq \iota_i \|\xi_i(k-1)\| + \iota_i \|\Delta \tilde{u}_{i_b}\| + \bar{\delta}_{1i} + \iota_i \bar{\delta}_{2i} \\ &\leq \iota_i^2 \|\xi_i(k-2)\| + (\iota_i^2 + \iota_i) \|\Delta \tilde{u}_{i_b}\| + (\iota_i + 1)(\bar{\delta}_{1i} + \iota_i \bar{\delta}_{2i}) \\ &\leq \dots \\ &\leq \iota_i^k \|\xi_i(0)\| + \frac{\bar{\delta}_{1i} + \iota_i \bar{\delta}_{2i}}{1 - \iota_i} + \frac{\iota_i \|\Delta \tilde{u}_{i_b}\|}{1 - \iota_i} \\ &\leq \iota_i^k \|\xi_i(0)\| + \frac{\bar{\delta}_{1i} + \iota_i \bar{\delta}_{2i}}{1 - \iota_i} + \frac{2\iota_i \beta}{1 - \iota_i} := \bar{\xi}_i. \end{aligned} \quad (31)$$

As $k \rightarrow \infty$, $\bar{\xi}_i \rightarrow \frac{\bar{\delta}_{1i} + \iota_i \bar{\delta}_{2i}}{1 - \iota_i} + \frac{2\iota_i \beta}{1 - \iota_i}$. This concludes the proof. \square

Theorem 1. Consider the system (12) with a sufficiently high sampling rate, if there exists a scalar $\bar{c}_i \in \mathbb{R}^+$ such that the following inequality is satisfied

$$\bar{\xi}_i < \bar{c}_i \|\Delta u_{i_b}\|, \quad (32)$$

the optimal incremental control policy (19) regulates the tracking error to a small neighbourhood around zero while minimizing the value function (14).

Proof. Considering that $V_i^*(e_i = 0) = 0$, and $V_i^* > 0$ for $\forall e_i \neq 0$, V_i^* in (16) could serve as a candidate Lyapunov function. Taking time derivative of V_i^* along the i -th incremental error subsystem (12) yields

$$\dot{V}_i^* = \nabla V_i^* (A_i e_i + B_i \Delta u_{i_b}^*) + \nabla V_i^* B_i \xi_i. \quad (33)$$

According to (17) and (18), the following equations establish

$$\begin{aligned} \nabla V_i^* (A_i e_i + B_i \Delta u_{i_b}^*) &= -e_i^\top Q_i e_i - W_i(\Delta u_{i_b}^*) - \bar{\xi}_{oi}^2 \\ \nabla V_i^* B_i &= -2\beta \tanh^{-1}(\Delta u_{i_b}^* / \beta). \end{aligned} \quad (34)$$

Substituting (34) into (33) yields

$$\dot{V}_i^* = -e_i^\top Q_i e_i - W_i(\Delta u_{i_b}^*) - \bar{\xi}_{oi}^2 - 2\beta \tanh^{-1}(\Delta u_{i_b}^* / \beta) \xi_i. \quad (35)$$

As for the $W_i(\Delta u_{i_b}^*)$ in (35), according to our previous result [19, Theorem 1], it follows that

$$W_i(\Delta u_{i_b}^*) = \beta^2 \sum_{j=1}^m (\tanh^{-1}(\Delta u_{i_b}^* / \beta))^2 - \epsilon_{ui}, \quad (36)$$

where $\epsilon_{u_i} \leq \frac{1}{2} \bar{g}_i^2 \nabla V_i^*{}^\top \nabla V_i^*$. Given that there exists $b_{\nabla V_i^*} \in \mathbb{R}^+$ such that $\|\nabla V_i^*\| \leq b_{\nabla V_i^*}$. Thus, we could rewrite the bound of ϵ_{u_i} as $\epsilon_{u_i} \leq b_{\epsilon_{u_i}} \leq \frac{1}{2} \bar{g}_i^2 b_{\nabla V_i^*}^2$.

Then, substituting (36) into (35), we get

$$\dot{V}_i^* = -e_i^\top Q_i e_i - [\beta \tanh^{-1}(\Delta u_{i_b}^*/\beta) + \xi_i]^2 - (\bar{\xi}_{oi}^2 - \xi_i^\top \xi_i) + b_{\epsilon_{u_i}}. \quad (37)$$

We choose $\bar{\xi}_{oi} = \bar{c}_i \|\Delta u_{i_b}\|$, and \bar{c}_i is picked to satisfy $\bar{c}_i \|\Delta u_{i_b}\| > \bar{\xi}_i$, where $\bar{\xi}_i$ is defined in (31). Then, the following equation holds

$$\dot{V}_i^* \leq -e_i^\top Q_i e_i + b_{\epsilon_{u_i}}. \quad (38)$$

Thus, if $-\lambda_{\min}(Q_i) \|e_i\|^2 + b_{\epsilon_{u_i}} < 0$, $\dot{V}_i^* < 0$ holds. Here $\lambda_{\min}(\cdot)$ denotes the minimum eigenvalues of a symmetric real matrix. Finally, it concludes that states of the i -th incremental error subsystem (12) converges to the residual set

$$\Omega_{e_i} = \{e_i \mid \|e_i\| \leq \sqrt{b_{\epsilon_{u_i}}/\lambda_{\min}(Q_i)}\}. \quad (39)$$

This concludes the proof. \square

Theorem 1 implies that the optimal incremental control policy $\Delta u_{i_b}^*$ (19) robustly stabilize (12). It has been clarified in Section 4.1 that the sub-RORCP of (12) equals to the sub-OTCP of (7). Thus, the designed $\Delta u_{i_b}^*$ and Δu_{i_f} solves the sub-OTCP of (7) together.

Remark 3. Here we offer guidelines to choose the values of \bar{g}_i required in Δu_{i_f} (10) and $\Delta u_{i_b}^*$ (19), which are critical to the effectiveness of our proposed tracking control scheme. According to [26], it is reasonable to assume that $\underline{m}_i \leq M_{ii} \leq \bar{m}_i$, where $\underline{m}_i, \bar{m}_i \in \mathbb{R}^+$. According to (3), $g_i = \frac{1}{M_{ii}}$. Thus, $\frac{1}{\bar{m}_i} \leq g_i \leq \frac{1}{\underline{m}_i}$ holds. To achieve $\|1 - g_i(k) \bar{g}_i^{-1}\| < 1$ required in (31), $\bar{g}_i > \frac{1}{2} g_i$ needs to be satisfied. Therefore, practitioners could choose $\bar{g}_i > \frac{1}{2 \underline{m}_i}$. The prior knowledge of M_{ii} provides designers with hints to choose a suitable \bar{g}_i .

5 Approximate solutions

This section uses a parallel critic learning structure to seek for the approximate solutions to the HJB equations (18) of n incremental error subsystems (12), which are difficult to solve directly. By reinvestigating the online NN weight learning process from a parameter identification perspective, we develop a simple yet efficient off-policy critic NN weight update law with guaranteed weight convergence by exploiting realtime and experience data together.

5.1 Value function approximation

For $e_i \in \Omega$, where $\Omega \subset \mathbb{R}^n$ is a compact set, the optimal value function (16) is approximated by an critic agent as [25]

$$V_i^* = W_i^{*\top} \Phi_i(e_i) + \epsilon_i(e_i), \quad (40)$$

where $W_i^* \in \mathbb{R}^{N_i}$ is the critic NN weight, $\Phi_i(e_i) : \mathbb{R}^2 \rightarrow \mathbb{R}^{N_i}$ represents the activation function, and $\epsilon_i(e_i) \in \mathbb{R}$ denotes the approximation error.

Remark 4. The utilized decoupled control technique in Section 3 solves the curse of complexity problem in (40). In particular, the constructed critic NN (40) relies on the error $e_i \in \mathbb{R}^2$ of the incremental error subsystem (13). The 2-D e_i allows us to construct a low-dimensional $\Phi_i(e_i)$ (easy to choose)² to approximate its associated V_i^* regardless of the value of the system dimension n . Otherwise, for a global approximation, i.e., $V^* = W^{*\top} \Phi(e) + \epsilon(e)$ with $e = x - x_d \in \mathbb{R}^{2n}$, the dimension of $\Phi(e)$ increases exponentially as n increases.

Given a fixed incremental control input Δu_{i_b} , combining (18) with (40) yields

$$W_i^{*\top} \nabla \Phi_i(A_i e_i + B_i \Delta u_{i_b}) + r_i(e_i, \Delta u_{i_b}) = \epsilon_{h_i}, \quad (41)$$

where the residual error follows $\epsilon_{h_i} = -\nabla \epsilon_i^\top (A_i e_i + B_i \Delta u_{i_b}) \in \mathbb{R}$. The NN parameterized (41) can be written into a linear in parameter (LIP) form as

$$\Theta_i = -W_i^{*\top} Y_i + \epsilon_{h_i}, \quad (42)$$

where $\Theta_i = r_i(e_i, \Delta u_{i_b}) \in \mathbb{R}$, and $Y_i = \nabla \Phi_i(A_i e_i + B_i \Delta u_{i_b}) \in \mathbb{R}^{N_i}$. This formulated LIP form (42) enables the learning of W_i^* to be equivalent to a parameter identification problem of a LIP system, which facilitates the development of an efficient weight update law in the subsequent subsection.

²It is displayed in Section 6 and Section 7 that 4-D activation functions $\Phi_i(e_i)$ in a fixed structure are chosen for subsystems of a 6-DoF quadrotor, 2-DoF and 3-DoF robot manipulators.

5.2 Off-policy critic NN weight update law

An approximation of (42) follows

$$\hat{\Theta}_i = -\hat{W}_i^\top Y_i, \quad (43)$$

where $\hat{W}_i \in \mathbb{R}^{N_i}$, $\hat{\Theta}_i \in \mathbb{R}$ are estimates of W_i^* and Θ_i , respectively. To achieve $\hat{W}_i \rightarrow W_i^*$, we design an off-policy critic NN weight update law for each subsystem as

$$\dot{\hat{W}}_i = -\Gamma_i k_{t_i} Y_i \tilde{\Theta}_i - \sum_{l=1}^{P_i} \Gamma_i k_{e_i} Y_{i_l} \tilde{\Theta}_{i_l}, \quad (44)$$

to update the critic NN weight \hat{W}_i in a parallel way to minimize $E_i = \frac{1}{2} \tilde{\Theta}_i^\top \tilde{\Theta}_i$, where $\tilde{\Theta}_i = \Theta_i - \hat{\Theta}_i \in \mathbb{R}$. Here $\Gamma_i \in \mathbb{R}^{N_i \times N_i}$ is a constant positive definite gain matrix; $k_{t_i}, k_{e_i} \in \mathbb{R}^+$ are used to trade-off the contribution of realtime and experience data to the online NN weight learning process; $P_i \in \mathbb{R}^+$ is the number of utilized recorded experience data.

To guarantee the weight convergence of (44), as proved in Theorem 2, the exploited experience data should be sufficient rich to satisfy the rank condition in Assumption 1, which can be easily satisfied by sequentially reusing experience data.

Assumption 1. Given an experience buffer $\mathfrak{B}_i = [Y_{i_1}, \dots, Y_{i_{P_i}}] \in \mathbb{R}^{N_i \times P_i}$, there holds $\text{rank}(\mathfrak{B}_i) = N_i$.

Theorem 2. Given Assumption 1, the NN weight learning error \tilde{W} converges to a small neighbourhood around zero.

Proof. The proof is similar to our previous work [19, Theorem 1]. Thus, it is omitted here due to page limits. \square

The guaranteed weight convergence of \hat{W}_i to W_i^* in Theorem 2 permits us to use a computation-simple single critic NN structure for each subsystem, where the estimated critic NN weight \hat{W}_i is directly used to construct the approximate optimal incremental control strategy:

$$\Delta \hat{u}_{i_b} = -\beta \tanh\left(\frac{1}{2\beta} B_i^\top \nabla \Phi_i^\top \hat{W}_i\right). \quad (45)$$

Finally, combining with (8), (10), and (45), we get the overall control input applied at the i -th subsystem (3)

$$\hat{u}_i = u_{i,0} + \Delta u_{i_f} + \Delta \hat{u}_{i_b}. \quad (46)$$

Based on the theoretical analysis mentioned above, we provide the main conclusions in Theorem 3.

Theorem 3. Given Assumption 1, for a sufficiently large N_i , the off-policy critic NN weight update law (44), and the approximate optimal incremental control policy (45) guarantee the tracking error and the NN weight learning error uniformly ultimately bounded (UUB).

Proof. See Appendix A. \square

6 Numerical simulation

This section first presents comparative simulations on a 2-DoF robot manipulator to show the superiority of our developed model-free IADP based tracking control scheme over the common model-based ADP based tracking control method [5] (for simplicity, referred to as CADP). Then, we numerically validate the efficiency of our proposed tracking control scheme on a 6-DoF quadrotor [27] trajectory tracking scenario.

6.1 Validation on a 2-DoF robot manipulator

The dynamics of a 2-DoF robot manipulator follows [5]

$$M(q)\ddot{q} + C(q, \dot{q})\dot{q} + F_d\dot{q} + F_s = \tau,$$

where $q = [q_1, q_2]^\top$, $\dot{q} = [\dot{q}_1, \dot{q}_2]^\top$, $\tau \in \mathbb{R}^2$; Let $c_2 = \cos q_2$, $s_2 = \sin q_2$, then $M(q) = \begin{bmatrix} a_1 + 2a_3c_2 & a_2 + a_3c_2 \\ a_2 + a_3c_2 & a_2 \end{bmatrix} \in \mathbb{R}^{2 \times 2}$, and $C(q, \dot{q}) = \begin{bmatrix} -a_3\dot{q}_2s_2 & -a_3(\dot{q}_1 + \dot{q}_2)s_2 \\ a_3\dot{q}_1s_2 & 0 \end{bmatrix} \in \mathbb{R}^{2 \times 2}$, $a_1 = 3.473 \text{ kg m}^2$, $a_2 = 0.196 \text{ kg m}^2$, $a_3 =$

0.242 kg m²; The static friction follows $F_d = \text{diag}[5.3, 1.1] \text{ N m s}$, and the dynamic friction is $F_s = [8.45 \tanh(\dot{q}_1), 2.35 \tanh(\dot{q}_2)]^\top \text{ N m s}$.

The considered OTCP is to design a control input τ to enable the state $x = [q_1, q_2, \dot{q}_1, \dot{q}_2]^\top$ to perfectly follow the desired trajectory $x_d = [k_{p1} \cos(t), k_{p2} \cos(t), -k_{p1} \sin(t), -k_{p2} \sin(t)]^\top$, where $k_{p1} = 0.5, k_{p2} = 1$ for $t \in [0, \frac{61\pi}{2})$, and $k_{p1} = 0.25, k_{p2} = 0.5$ for $t \in [\frac{61\pi}{2}, 400]$. This adopted piecewise trajectory x_d violates the Assumption 2 in [5] that the desired trajectory is generated from one assumed reference trajectory dynamics. A simple varying x_d (only the amplitude changes into a half value) serves as an example to show the learning inefficiency of CADP based tracking control scheme under varying desired trajectories.

To achieve an accurate value function approximation, we implement the CADP method by using a 23-D activation function provided in [5] but adopting our proposed weight update law (44) to achieve a fair comparison³. The 23-D activation function is provided here for completeness:

$$\begin{aligned} \Phi(\rho) = & \frac{1}{2}[\rho_1^2, \rho_2^2, 2\rho_1\rho_3, 2\rho_1\rho_4, 2\rho_2\rho_3, 2\rho_2\rho_4, \rho_1^2\rho_5^2, \rho_1^2\rho_6^2, \rho_1^2\rho_7^2, \\ & \rho_1^2\rho_8^2, \rho_1^2\rho_9^2, \rho_1^2\rho_{10}^2, \rho_2^2\rho_5^2, \rho_2^2\rho_6^2, \rho_2^2\rho_7^2, \rho_2^2\rho_8^2, \rho_2^2\rho_9^2, \rho_2^2\rho_{10}^2, \\ & \rho_3^2\rho_5^2, \rho_3^2\rho_6^2, \rho_3^2\rho_7^2, \rho_3^2\rho_8^2, \rho_3^2\rho_9^2, \rho_3^2\rho_{10}^2, \rho_4^2\rho_5^2, \rho_4^2\rho_6^2, \rho_4^2\rho_7^2, \rho_4^2\rho_8^2, \rho_4^2\rho_9^2, \rho_4^2\rho_{10}^2]^\top. \end{aligned}$$

where $\rho = [e^\top, x_d^\top]^\top \in \mathbb{R}^8$, $e = x - x_d \in \mathbb{R}^4$. Our developed IADP approach adopts 4-D activation functions $\Phi_i(e_i) = [e_{i1}^2, e_{i2}^2, e_{i1}e_{i2}, e_{i2}^3]^\top$, $i = 1, 2$, for the decoupled subsystem 1 and 2. The utilized low-dimensional activation functions $\Phi_i(e_i)$ in a fixed structure exemplify IADP's scalability and practicability. The detailed parameter settings for CADP and IADP based tracking control schemes are provided in Table 1.

Table 1: The parameter settings of different methods.

	CADP [5]	IADP
Initial value	$x(0) = [0.5, 1.1, 0, 0]^\top$,	$x(0) = [0.5, 1.1, 0, 0]^\top$,
conditions	$x_d(0) = [0.5, 1, 0, 0]^\top$,	$u(0) = [0, 0]^\top, \bar{g}_i = 7,$
	$u(0) = [0, 0]^\top$,	$\hat{W}_i(0) = 0_{4 \times 1}, k_{i1} = 10,$
	$\hat{W}(0) = 0_{23 \times 1}$.	$k_{i2} = 10, i = 1, 2.$
Cost function parameters	$Q = \text{diag}(600, 600, 1, 1),$	$Q_i = \text{diag}(600, 1),$
	$R = \text{diag}(1, 1).$	$\beta = 0.1, \bar{c}_i = 29, i = 1, 2.$
Weight learning parameters	$k_t = 80, k_h = 1, P = 25,$	$k_{t_i} = 80, k_{e_i} = 1, P_i = 12,$
	$\Gamma = \text{diag}(I_{1 \times 23}).$	$\Gamma_i = \text{diag}(I_{1 \times 4}), i = 1, 2.$

As displayed in Fig.2a and Fig.2b, both CADP and IADP based tracking control strategies achieve a satisfying performance in the first period $t \in [0, \frac{61\pi}{2})$. However, when the desired trajectory changes at $\frac{61\pi}{2}$ s, the learning inefficiency of the CADP based tracking control scheme (with fine-tuned hyperparameters) hinders us from getting a high-precision tracking performance but with steady-state errors. Our proposed tracking control scheme efficiently drives the robot manipulator to track the varying desired trajectories accurately. The estimated weight trajectories of two methods are displayed in Fig.3. Although both CADP and IADP based tracking control schemes achieve weight convergence in the first period, however, the weight convergence is lost for the CADP method when the reference trajectory changes, as displayed in Fig.3a. The weight convergence result of subsystem 2 provided in Fig.3b serves as a representative example to show the learning efficiency of IADP based tracking control scheme. In summary, our developed IADP based model-free tracking control scheme achieves performance competitive with model-based CADP method, and enjoys better scalability to value function approximation and flexibility to varying desired trajectories.

6.2 Validation on a 6-DoF quadrotor

This subsection further certifies the effectiveness of IADP based tracking control scheme under a high-dimensional quadrotor tracking task. The quadrotor [27] is driven to track the desired spiral reference trajectory $x_r = [\frac{3}{10 \sin(t)}, \cos(t), \frac{t}{10\pi}, 0]^\top \in \mathbb{R}^3$, $t \in [0, 50]$. The associated parameter settings to conduct numerical simulations are referred to Table 2. The detailed procedures to decouple the 6-DoF quadrotor into 6 subsystems (3) are referred to Appendix B. For subsystem 1-6, we adopt the same activation functions used in Section 6.1. As displayed in Fig.4, we obtain a satisfying tracking performance via the IADP based tracking control scheme.

³The weight update law proposed in [5] requires to directly add probing noise to control inputs to meet the required PE condition for the weight convergence, which causes undesirable oscillations.

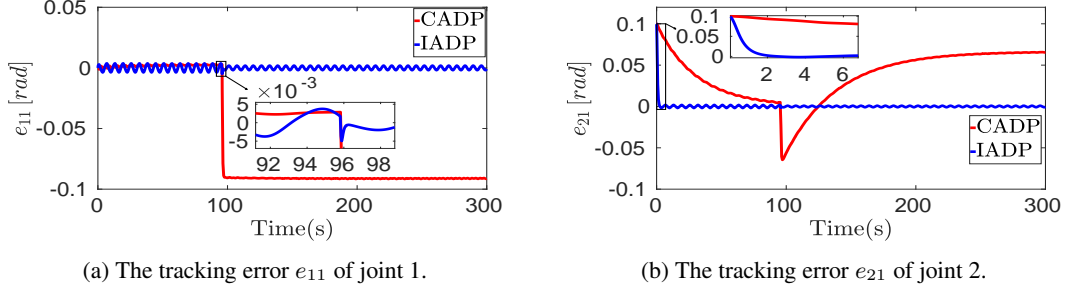


Figure 2: The comparison of tracking error trajectories.

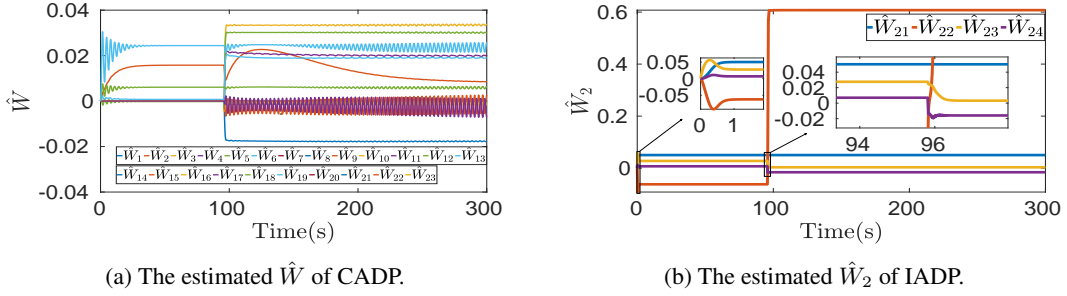


Figure 3: The comparison of estimated weight trajectories.

Table 2: The parameter settings of a quadrotor OTCP.

Initial value	$\xi(0) = [0.1, 1.1, 0]^T, \eta(0) = [0, 0, 0]^T, u(0) = [0, 0, 0.5]^T,$
conditions	$\bar{g}_i = 300, i = 1, 2, 3; \bar{g}_i = 60000, i = 4, 5, 6, k_{i_1} = 3, k_{i_2} = 3, \hat{W}_i(0) = 0_{4 \times 1}, i = 1, \dots, 6.$
Cost function parameters	$Q_i = \text{diag}(1, 1), \bar{c}_i = 4, \beta = 0.1, i = 1, \dots, 6.$
Weight learning parameters	$k_{t_i} = 1, k_{e_i} = 0.01, P_i = 6, \Gamma_i = 0.01 \text{diag}(I_{1 \times 4}), i = 1, \dots, 6.$

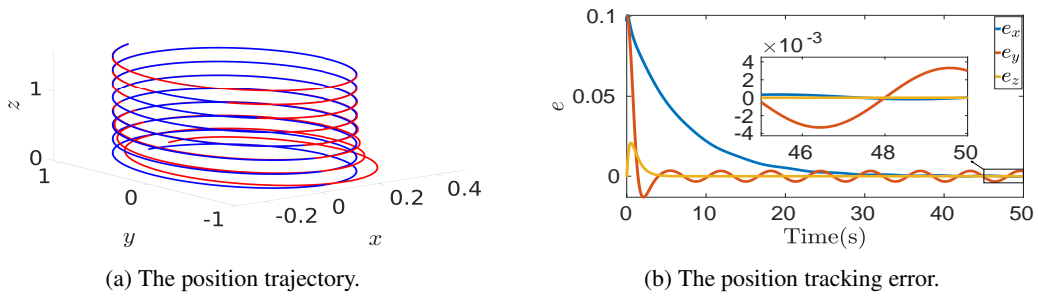


Figure 4: The position tracking performance of a quadrotor.

7 Experimental validation

This section experimentally validates the efficiency of our proposed tracking control scheme on a 3-DoF robot manipulator (see Fig.5). The executable algorithm is created by MATLAB 2017a in Ubuntu 14.04 LTS with the first-order Euler solver at the sampling rate of 1kHz. The measured angular position is numerically differentiated to compute the angular velocity and acceleration of the robot [20]. The E-L equation follows

$$M(q)\ddot{q} + N(q, \dot{q})\dot{q} = \tau,$$

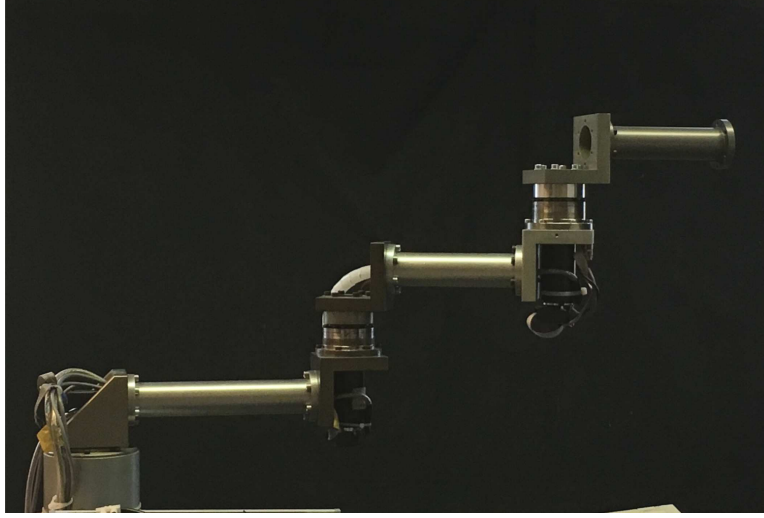


Figure 5: 3-DoF robot manipulator for experimental validation.

where $q, \dot{q}, \tau \in \mathbb{R}^3$. The explicit forms of $M(q), N(q, \dot{q}) \in \mathbb{R}^{3 \times 3}$ are referred to [28]. During the experiment ⁴, the robot manipulator is driven to track the desired piecewise trajectory $x_d = [q_d^\top, \dot{q}_d^\top]^\top \in \mathbb{R}^6$ with $q_d = (1 + \sin(\frac{t}{2} - \frac{\pi}{2}))k_{p3} \in \mathbb{R}^3$, where $k_{p3} = [0.3, 0.6, 1]^\top$ for $t \in [0, 5)$, and $k_{p3} = [0.2, 0.5, 0.8]^\top$ for $t \in [5, 10]$.

The activation functions $\Phi_i(e_i), i = 1, 2, 3$, for value function approximation are the same with ones picked in Section 6.1. Given the sampling rate is 1kHz, accordingly, we choose the delay time as $L = 0.001$ s. The parameters for subsystem 1-3 are set as: $Q_i = \text{diag}[300, 40000]$, $\bar{c}_i = 200$, $\Gamma_i = \text{diag}[100, 4, 0.1, 16]$, $k_{t_i} = 0.2$, $k_{h_i} = 0.01$, $P_i = 10$, $k_{i_1} = 8$, $k_{i_2} = 8$, $i = 1, 2, 3$; and $\beta = 0.1$, $\bar{g}_1 = 40$, $\bar{g}_2 = 46$, and $\bar{g}_3 = 54$.

The trajectories of $e_{i_1}, i = 1, 2, 3$ under different payloads (installed to the end effector of the robot manipulator) are displayed in Fig.6a, Fig.6c, and Fig.6e, respectively. It is shown that our developed tracking control scheme efficiently track the desired trajectories with a satisfying tracking precision and robustness against varying payloads. The evolution trajectories of \hat{W}_i for the 500g payload case, which are trained in parallel using realtime and experience data together, are displayed in Fig.6b, Fig.6d, and Fig.6f, respectively. We obtain the desired weight convergence for three subsystems. This validate the realtime learning performance of our developed weight update law (44).

To further show the superiority of IADP based tracking control scheme under different tasks, we drive the end effector of the robot manipulator to track three different reference circles in task space sequentially. Circle 1: center $c_1 = (0.69, 0.05)$ and radius as $r_1 = 0.2$; Circle 2: center $c_2 = (0.72, 0.05)$ and radius as $r_2 = 0.16$; Circle 3: center $c_3 = (0.75, 0.05)$ and radius as $r_3 = 0.12$. We use the Robotics toolbox [29] to conduct the inverse kinematics calculation to get the associated joint space trajectories of Circle 1-3, which are inputs of our proposed IADP based tracking control scheme. The required joint lengths to conduct the inverse kinematics calculation are $l_1 = 0.3$ m, $l_2 = 0.24$ m, $l_3 = 0.34$ m. More details of experimental settings are referred to Table 3. The associated tracking trajectories in joint

Table 3: The parameter settings for the IADP method.

Initial value conditions	$x(0) = [0, 0, 0, 0]^\top, u(0) = [0, 0]^\top,$ $\bar{g}_1 = 14, \bar{g}_2 = 32, \bar{g}_3 = 80,$ $k_{i_1} = 8, k_{i_2} = 8, \hat{W}_i(0) = 0_{4 \times 1}, i = 1, 2, 3$
Cost function parameters	$Q_1 = \text{diag}(16, 10), Q_2 = \text{diag}(18, 10),$ $Q_3 = \text{diag}(0.2, 0.1), \beta = 1, \bar{c}_i = 4, i = 1, 2, 3$
Weight learning parameters	$k_{t_i} = 1, k_{e_i} = 1, P_i = 10, i = 1, 2, 3$ $\Gamma_1 = 0.001 \text{diag}(I_{1 \times 4}), \Gamma_2 = 0.003 \text{diag}(I_{1 \times 4}),$ $\Gamma_3 = 0.001 \text{diag}(I_{1 \times 4}).$

⁴The CADP based tracking control scheme is impractical to conduct the experimental validation on a 3-DoF robot manipulator. A high-dimensional activation function is required to approximate the value function of the constructed 12-D augmented system [5]. It is not trivial. Even though a high-dimensional activation function is available, the realtime performance of the corresponding weight update law is poor for practical experiments.

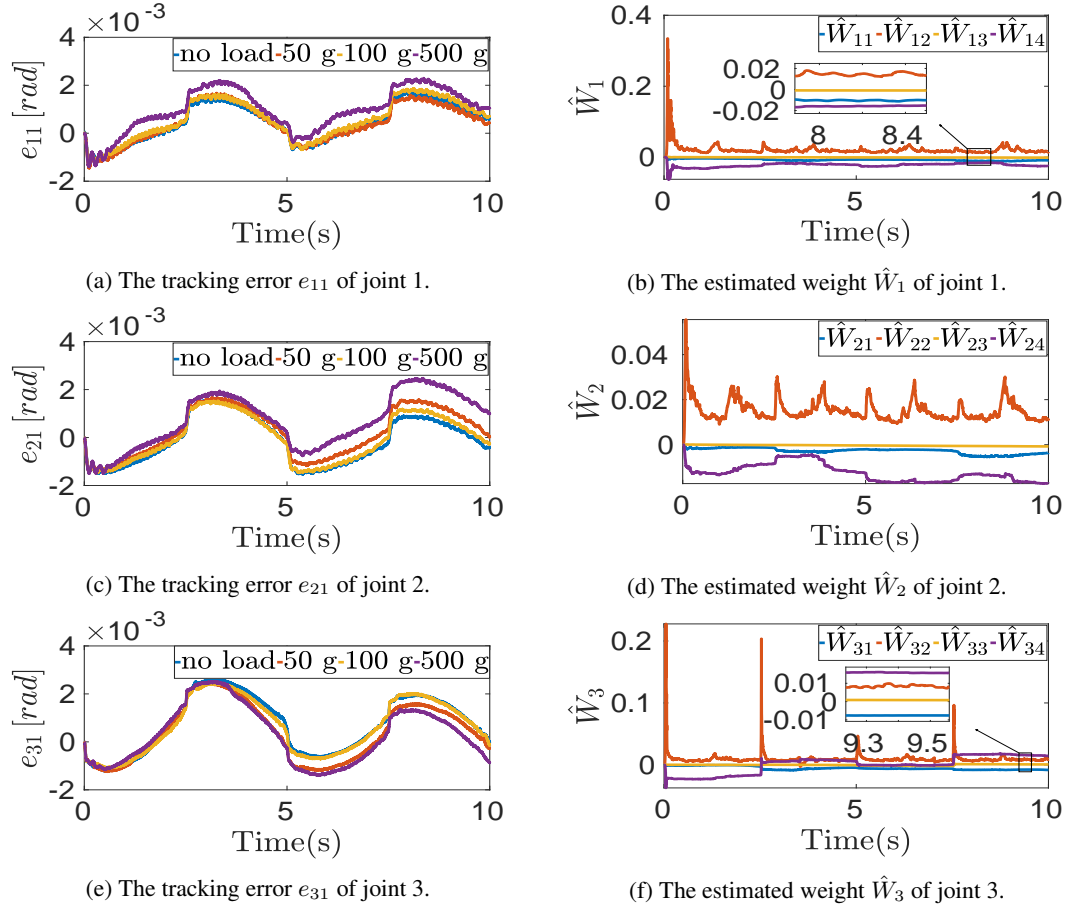


Figure 6: The trajectories of the tracking error e_{i1} and the estimated weight \hat{W}_i under different payloads, $i = 1, 2, 3$.

space and task space are displayed in Fig.7 and Fig.8, respectively. The satisfying tracking performance validates the efficiency of IADP based tracking control scheme. The weight convergence result of three subsystems displayed in Fig.9 validates the effectiveness of our proposed weight update law (44).

8 Conclusion

This paper develops an IADP based tracking control scheme to address the limitations of existing ADP based solutions to the OTCP. Through decoupled control and TDE techniques, the investigated OTCP of a high-dimensional system is divided into multiple sub-OTCPs of incremental subsystems. Then, the sub-OTCPs are transformed into sub-RORCPs that are approximately solved by IADP. Simulation and experimental results validate that our proposed model-free tracking control strategy could be applied to a high-dimensional system with the flexibility of different tracking tasks. However, the input saturation is not addressed in the current work, which remains our future work.

Acknowledgment

The authors would like to thank Ahmed Nesrin for helping conduct numerical and experimental validations.

References

- [1] Dimitri P Bertsekas. *Dynamic programming and optimal control*, volume 1. Athena scientific Belmont, MA, 1995.
- [2] Frank L Lewis, Draguna Vrabie, and Vassilis L Syrmos. *Optimal control*. John Wiley & Sons, 2012.

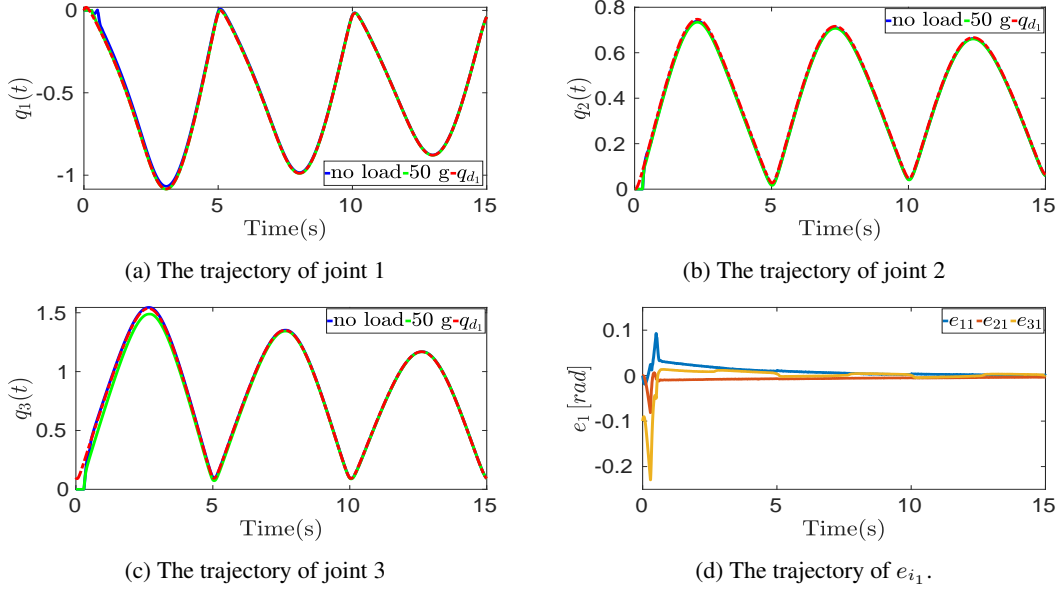


Figure 7: The joint space trajectories under different payloads.

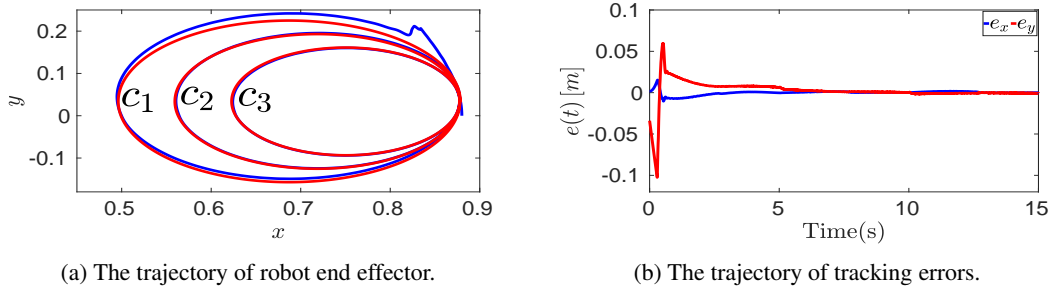


Figure 8: The task space trajectories of the circle tracking scenario.

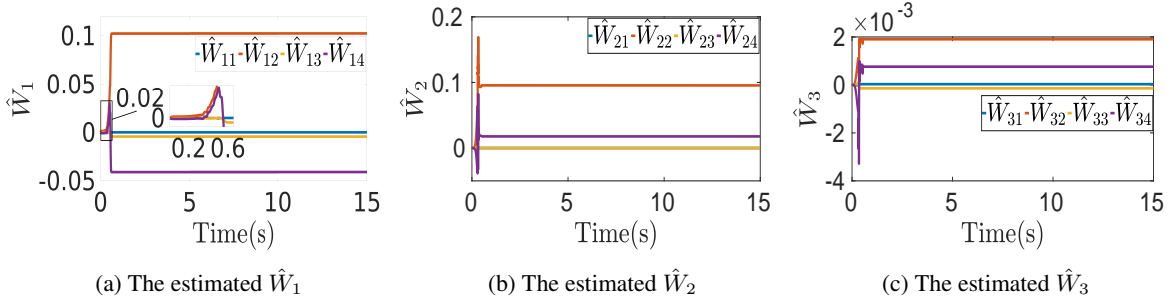


Figure 9: The evolution trajectory of the estimated weights.

- [3] Bahare Kiumarsi, Kyriakos G Vamvoudakis, Hamidreza Modares, and Frank L Lewis. Optimal and autonomous control using reinforcement learning: A survey. *IEEE transactions on neural networks and learning systems*, 29(6):2042–2062, 2017.
- [4] Rushikesh Kamalapurkar, Joel A Rosenfeld, and Warren E Dixon. Efficient model-based reinforcement learning for approximate online optimal control. *Automatica*, 74:247–258, 2016.
- [5] Rushikesh Kamalapurkar, Huyen Dinh, Shubhendu Bhasin, and Warren E Dixon. Approximate optimal trajectory tracking for continuous-time nonlinear systems. *Automatica*, 51:40–48, 2015.
- [6] Huaguang Zhang, Lili Cui, Xin Zhang, and Yanhong Luo. Data-driven robust approximate optimal tracking con-

-
- trol for unknown general nonlinear systems using adaptive dynamic programming method. *IEEE Transactions on Neural Networks*, 22(12):2226–2236, 2011.
- [7] Hamidreza Modares and Frank L Lewis. Optimal tracking control of nonlinear partially-unknown constrained-input systems using integral reinforcement learning. *Automatica*, 50(7):1780–1792, 2014.
 - [8] Wanbing Zhao, Hao Liu, and Frank L Lewis. Robust formation control for cooperative underactuated quadrotors via reinforcement learning. *IEEE Transactions on Neural Networks and Learning Systems*, 2020.
 - [9] Rushikesh Kamalapurkar, Lindsey Andrews, Patrick Walters, and Warren E Dixon. Model-based reinforcement learning for infinite-horizon approximate optimal tracking. *IEEE transactions on neural networks and learning systems*, 28(3):753–758, 2016.
 - [10] Yanbin Liu, Weichao Sun, and Huijun Gao. High precision robust control for periodic tasks of linear motor via b-spline wavelet neural network observer. *IEEE Transactions on Industrial Electronics*, 2021.
 - [11] Yongming Li, Kangkang Sun, and Shaocheng Tong. Observer-based adaptive fuzzy fault-tolerant optimal control for siso nonlinear systems. *IEEE transactions on cybernetics*, 49(2):649–661, 2018.
 - [12] Thomas Beckers, Jonas Umlauf, Dana Kulic, and Sandra Hirche. Stable gaussian process based tracking control of lagrangian systems. In *2017 IEEE 56th Annual Conference on Decision and Control (CDC)*, pages 5180–5185. IEEE, 2017.
 - [13] Jing Na, Guido Herrmann, and Kyriakos G Vamvoudakis. Adaptive optimal observer design via approximate dynamic programming. In *2017 American Control Conference (ACC)*, pages 3288–3293. IEEE, 2017.
 - [14] Bruce A Finlayson. *The method of weighted residuals and variational principles*, volume 73. SIAM, 2013.
 - [15] Murad Abu-Khalaf and Frank L Lewis. Nearly optimal control laws for nonlinear systems with saturating actuators using a neural network hjb approach. *Automatica*, 41(5):779–791, 2005.
 - [16] Bo Sun and Erik-Jan van Kampen. Reinforcement-learning-based adaptive optimal flight control with output feedback and input constraints. *Journal of Guidance, Control, and Dynamics*, pages 1–8, 2021.
 - [17] Michael Lutter, Boris Belousov, Kim Listmann, Debora Clever, and Jan Peters. Hjb optimal feedback control with deep differential value functions and action constraints. In *Conference on Robot Learning*, pages 640–650. PMLR, 2020.
 - [18] Kamal Youcef-Toumi and S-T Wu. Input/output linearization using time delay control. 1992.
 - [19] Cong Li, Yongchao Wang, Fangzhou Liu, Qingchen Liu, and Martin Buss. Model-free incremental adaptive dynamic programming based approximate robust optimal regulation. *arXiv preprint arXiv:2105.01698*, 2021.
 - [20] TC Steve Hsia. A new technique for robust control of servo systems. *IEEE Transactions on Industrial Electronics*, 36(1):1–7, 1989.
 - [21] Maolin Jin, Jinoh Lee, Pyung Hun Chang, and Chintae Choi. Practical nonsingular terminal sliding-mode control of robot manipulators for high-accuracy tracking control. *IEEE Transactions on Industrial Electronics*, 56(9):3593–3601, 2009.
 - [22] Bo Zhao and Derong Liu. Event-triggered decentralized tracking control of modular reconfigurable robots through adaptive dynamic programming. *IEEE Transactions on Industrial Electronics*, 67(4):3054–3064, 2019.
 - [23] Fangchao Luo, Bo Zhao, and Derong Liu. Event-triggered decentralized optimal fault tolerant control for mismatched interconnected nonlinear systems through adaptive dynamic programming. *Optimal Control Applications and Methods*, 2021.
 - [24] Lucian Buşoniu, Tim de Bruin, Domagoj Tolić, Jens Kober, and Ivana Palunko. Reinforcement learning for control: Performance, stability, and deep approximators. *Annual Reviews in Control*, 46:8–28, 2018.
 - [25] Kyriakos G Vamvoudakis and Frank L Lewis. Online actor–critic algorithm to solve the continuous-time infinite horizon optimal control problem. *Automatica*, 46(5):878–888, 2010.
 - [26] FW Lewis, Suresh Jagannathan, and Aydin Yesildirak. *Neural network control of robot manipulators and nonlinear systems*. CRC press, 2020.
 - [27] Marcus Greiff. Modelling and control of the crazyflie quadrotor for aggressive and autonomous flight by optical flow driven state estimation. 2017.
 - [28] Cong Li, Fangzhou Liu, Yongchao Wang, and Martin Buss. Concurrent learning-based adaptive control of an uncertain robot manipulator with guaranteed safety and performance. *IEEE Transactions on Systems, Man, and Cybernetics: Systems*, 2021.

-
- [29] Peter Corke. Robotics toolbox. *Obtained from Peter O. Corke site: <http://www.petercorke.com/Robotics%20Toolbox.html>, 2002.*
- [30] Xiong Yang, Derong Liu, Hongwen Ma, and Yancai Xu. Online approximate solution of hji equation for unknown constrained-input nonlinear continuous-time systems. *Information Sciences*, 328:435–454, 2016.

A Proof of Theorem 3

Assumption 2. [25] *There exist constants $b_{\epsilon_i}, b_{\epsilon_{ei}}, b_{\epsilon_{hi}}, b_{\Phi_i}, b_{\Phi_{ei}} \in \mathbb{R}^+$ such that $\|\epsilon_i(e_i)\| \leq b_{\epsilon_i}$, $\|\nabla \epsilon_i(e_i)\| \leq b_{\epsilon_{ei}}$, $\|\epsilon_{hi}\| \leq b_{\epsilon_{hi}}$, $\|\Phi_i(e_i)\| \leq b_{\Phi_i}$, and $\|\nabla \Phi_i(e_i)\| \leq b_{\Phi_{ei}}$.*

Proof. Consider the candidate Lyapunov function for the i -th incremental error subsystem (12) as

$$L_i = V_i^* + \frac{1}{2} \tilde{W}_i^\top \Gamma_i^{-1} \tilde{W}_i. \quad (47)$$

By denoting $L_{i1} = V_i^*$, its derivative follows

$$\begin{aligned} \dot{L}_{i1} &= \nabla V_i^{*\top} (A_i e_i + B_i \Delta \hat{u}_{ib} + B_i \xi_i) \\ &= \nabla V_i^{*\top} (A_i e_i + B_i \Delta u_{ib}^*) + \nabla V_i^{*\top} B_i \xi_i + \nabla V_i^{*\top} B_i (\Delta \hat{u}_{ib} - \Delta u_{ib}^*). \end{aligned} \quad (48)$$

Substituting (34) into (48) reads

$$\begin{aligned} \dot{L}_{i1} &= -e_i^\top Q_i e_i - \mathcal{W}(\Delta u_{ib}^*) - \bar{\xi}_{oi}^2 - 2\beta \tanh^{-1}(\Delta u_{ib}^*/\beta) \xi_i \\ &\quad - 2\beta \tanh^{-1}(\Delta u_{ib}^*/\beta) (\Delta \hat{u}_{ib} - \Delta u_{ib}^*). \end{aligned} \quad (49)$$

Combining with (36) and (37), (49) follows

$$\begin{aligned} \dot{L}_{i1} &\leq -e_i^\top Q_i e_i - (\bar{\xi}_{oi}^2 - \|\xi_i\|^2) - [\beta \tanh^{-1}(\Delta u_{ib}^*/\beta) + \xi_i]^2 \\ &\quad + \frac{1}{2} \nabla V_i^{*\top} B_i B_i^\top \nabla V_i^* - 2\beta \tanh^{-1}(\Delta u_{ib}^*/\beta) (\Delta \hat{u}_{ib} - \Delta u_{ib}^*). \end{aligned} \quad (50)$$

The term $-2\beta \tanh^{-1}(\Delta u_{ib}^*/\beta) (\Delta \hat{u}_{ib} - \Delta u_{ib}^*)$ in (50) follows

$$-2\beta \tanh^{-1}(\Delta u_{ib}^*/\beta) (\Delta \hat{u}_{ib} - \Delta u_{ib}^*) \leq \beta^2 \|\tanh^{-1}(\Delta u_{ib}^*/\beta)\|^2 + \|\Delta \hat{u}_{ib} - \Delta u_{ib}^*\|^2. \quad (51)$$

According to (19) and (40), and the mean-value theorem, the optimal incremental control is rewritten as

$$\Delta u_{ib}^* = -\beta \tanh\left(\frac{1}{2\beta} B_i^\top \nabla \Phi_i^\top W_i^*\right) - \epsilon_{\Delta u_i^*}, \quad (52)$$

where $\epsilon_{\Delta u_i^*} = \frac{1}{2}(1 - \tanh^2(\eta_i)) B_i^\top \nabla \epsilon_i$, and $\eta_i \in \mathbb{R}$ is chosen between $\frac{1}{2\beta} B_i^\top \nabla \Phi_i^\top W_i^*$ and $\frac{1}{2\beta} B_i^\top \nabla V_i^*$. According to $\|\nabla \epsilon_i\| \leq b_{\epsilon_{ei}}$ in Assumption 2, $\|\epsilon_{\Delta u_i^*}\| \leq \frac{1}{2} \|B_i\| b_{\epsilon_{ei}}$ holds. Then, by combining (45) with (52), we get

$$\Delta \hat{u}_{ib} - \Delta u_{ib}^* = \beta (\tanh(\mathcal{G}_i^*) - \tanh(\hat{\mathcal{G}}_i)) + \epsilon_{\Delta u_i^*}. \quad (53)$$

where $\mathcal{G}_i^* = \frac{1}{2\beta} B_i^\top \nabla \Phi_i^\top W_i^*$, and $\hat{\mathcal{G}}_i = \frac{1}{2\beta} B_i^\top \nabla \Phi_i^\top \tilde{W}_i$. Based on (19) and (45), the Taylor series of $\tanh(\mathcal{G}_i^*)$ follows

$$\begin{aligned} \tanh(\mathcal{G}_i^*) &= \tanh(\hat{\mathcal{G}}_i) + \frac{\partial \tanh(\hat{\mathcal{G}}_i)}{\partial \hat{\mathcal{G}}_i} (\mathcal{G}_i^* - \hat{\mathcal{G}}_i) + \mathcal{O}((\mathcal{G}_i^* - \hat{\mathcal{G}}_i)^2) \\ &= \tanh(\hat{\mathcal{G}}_i) - \frac{1}{2\beta} (1 - \tanh^2(\hat{\mathcal{G}}_i)) B_i^\top \nabla \Phi_i^\top \tilde{W}_i + \mathcal{O}((\mathcal{G}_i^* - \hat{\mathcal{G}}_i)^2), \end{aligned} \quad (54)$$

where $\mathcal{O}((\mathcal{G}_i^* - \hat{\mathcal{G}}_i)^2)$ is a higher order term of the Taylor series. By following [30, Lemma 1], this higher order term is bounded as

$$\|\mathcal{O}((\mathcal{G}_i^* - \hat{\mathcal{G}}_i)^2)\| \leq 2 + \frac{1}{\beta} \|B_i\| b_{\Phi_{ei}} \|\tilde{W}_i\|. \quad (55)$$

Based on (54), we rewrite (53) as

$$\begin{aligned} \Delta \hat{u}_{ib} - \Delta u_{ib}^* &= \beta (\tanh(\mathcal{G}_i^*) - \tanh(\hat{\mathcal{G}}_i)) + \epsilon_{\Delta u_i^*} \\ &= -\frac{1}{2} (1 - \tanh^2(\hat{\mathcal{G}}_i)) B_i^\top \nabla \Phi_i^\top \tilde{W}_i + \beta \mathcal{O}((\mathcal{G}_i^* - \hat{\mathcal{G}}_i)^2) + \epsilon_{\Delta u_i^*}. \end{aligned} \quad (56)$$

Then, by combining (55) with (56), and given that $\left\|1 - \tanh^2(\hat{\mathcal{G}}_i)\right\| \leq 2$, $\|\Delta \hat{u}_{i_b} - \Delta u_{i_b}^*\|^2$ in (51) follows

$$\begin{aligned} \|\Delta \hat{u}_{i_b} - \Delta u_{i_b}^*\|^2 &\leq 3\beta^2 \left\| \mathcal{O}((\mathcal{G}_i^* - \hat{\mathcal{G}}_i)^2) \right\|^2 + 3 \left\| \epsilon_{\Delta u_i^*} \right\|^2 + 3 \left\| -\frac{1}{2}(1 - \tanh^2(\hat{\mathcal{G}}_i)) B_i^\top \nabla \Phi_i^\top \tilde{W}_i \right\|^2 \\ &\leq 6 \|B_i\|^2 b_{\Phi_{ei}}^2 \left\| \tilde{W}_i \right\|^2 + 12\beta^2 + \frac{3}{4} \|B_i\|^2 b_{\epsilon_{ei}}^2 + 12\beta \|B_i\| b_{\Phi_{ei}} \left\| \tilde{W}_i \right\|. \end{aligned} \quad (57)$$

Based on (34), (40), Assumption 2, and the fact that $\|W_i^*\| \leq b_{W_i^*}$, $\|\tanh^{-1}(\Delta u_{i_b}^*/\beta)\|^2$ in (51) follows

$$\begin{aligned} \|\tanh^{-1}(\Delta u_{i_b}^*/\beta)\|^2 &= \left\| \frac{1}{4\beta^2} \nabla V_i^{*\top} B_i B_i^\top \nabla V_i^* \right\| \\ &\leq \frac{1}{4\beta^2} \|B_i\|^2 b_{\Phi_{ei}}^2 b_{W_i^*}^2 + \frac{1}{4\beta^2} b_{\epsilon_{ei}}^2 \|B_i\|^2 + \frac{1}{2\beta^2} \|B_i\|^2 b_{\Phi_{ei}} b_{\epsilon_{ei}} b_{W_i^*}. \end{aligned} \quad (58)$$

Using (57) and (58), (51) reads

$$\begin{aligned} &-2\beta \tanh^{-1}(\Delta u_{i_b}^*/\beta) (\Delta \hat{u}_{i_b} - \Delta u_{i_b}^*) \leq \frac{1}{4} \|B_i\|^2 b_{\Phi_{ei}}^2 b_{W_i^*}^2 \\ &+ \frac{1}{4} b_{\epsilon_{ei}}^2 \|B_i\|^2 + \frac{1}{2} \|B_i\|^2 b_{\Phi_{ei}} b_{\epsilon_{ei}} b_{W_i^*} + 6 \|B_i\|^2 b_{\Phi_{ei}}^2 \left\| \tilde{W}_i \right\|^2 \\ &+ 12\beta^2 + \frac{3}{4} \|B_i\|^2 b_{\epsilon_{ei}}^2 + 12\beta \|B_i\| b_{\Phi_{ei}} \left\| \tilde{W}_i \right\|. \end{aligned} \quad (59)$$

Substituting (59) into (50), finally the first term \dot{L}_{i_1} follows

$$\begin{aligned} \dot{L}_{i_1} &\leq -e_i^\top Q_i e_i - (\bar{\xi}_{oi}^2 - \xi_i^\top \xi_i) - [\beta \tanh^{-1}(\Delta u_{i_b}^*/\beta) + \xi_i]^2 \\ &+ \frac{3}{4} \|B_i\|^2 b_{\Phi_{ei}}^2 b_{W_i^*}^2 + \frac{3}{4} b_{\epsilon_{ei}}^2 \|B_i\|^2 + \frac{3}{2} \|B_i\|^2 b_{\Phi_{ei}} b_{\epsilon_{ei}} b_{W_i^*} \\ &+ 6 \|B_i\|^2 b_{\Phi_{ei}}^2 \left\| \tilde{W}_i \right\|^2 + 12\beta^2 + \frac{3}{4} \|B_i\|^2 b_{\epsilon_{ei}}^2 + 12\beta \|B_i\| b_{\Phi_{ei}} \left\| \tilde{W}_i \right\|. \end{aligned} \quad (60)$$

As for the second term $\dot{L}_W = \frac{1}{2} \tilde{W}_i^\top \Gamma_i^{-1} \tilde{W}_i$, based on (44) and Theorem 1 in our previous work [19], it follows

$$\dot{L}_{i_2} \leq -\tilde{W}_i^\top \mathcal{Y}_i \tilde{W}_i + \tilde{W}_i^\top \epsilon_{\tilde{W}_i}. \quad (61)$$

where $\mathcal{Y}_i = \sum_{l=1}^{P_i} k_{ei} Y_{il} Y_{il}^\top \in \mathbb{R}^{N_i \times N_i}$, and $\epsilon_{\tilde{W}_i} = -k_{ti} Y_i \epsilon_{hi} - \sum_{l=1}^{P_i} k_{ei} Y_{il} \epsilon_{hil} \in \mathbb{R}^{N_i}$. The boundness of Y_i and ϵ_{hi} results in bounded $\epsilon_{\tilde{W}_i}$. Thus, there exists $\bar{\epsilon}_{\tilde{W}_i} \in \mathbb{R}^+$ such that $\|\epsilon_{\tilde{W}_i}\| \leq \bar{\epsilon}_{\tilde{W}_i}$. According to Assumption 1, \mathcal{Y}_i is positive definite. Thus, (61) could be rewritten as

$$\dot{L}_{i_2} \leq -\lambda_{\min}(\mathcal{Y}_i) \left\| \tilde{W}_i \right\|^2 - \bar{\epsilon}_{\tilde{W}_i} \left\| \tilde{W}_i \right\|. \quad (62)$$

Finally, as for \dot{L}_i , substituting (60) and (61) into (47), we get

$$\dot{L}_i \leq -\mathcal{A}_i - \mathcal{B}_i \left\| \tilde{W}_i \right\|^2 + \mathcal{C}_i \left\| \tilde{W}_i \right\| + \mathcal{D}_i, \quad (63)$$

where $\mathcal{A}_i = e_i^\top Q_i e_i + (\bar{\xi}_{oi}^2 - \xi_i^\top \xi_i) + [\beta \tanh^{-1}(\Delta u_{i_b}^*/\beta) + \xi_i]^2$, $\mathcal{B}_i = \lambda_{\min}(\mathcal{Y}_i) - 6 \|B_i\|^2 b_{\Phi_{ei}}^2$, $\mathcal{C}_i = 12\beta \|B_i\| b_{\Phi_{ei}} + \bar{\epsilon}_{\tilde{W}_i}$, and $\mathcal{D}_i = \frac{3}{4} \|B_i\|^2 b_{\Phi_{ei}}^2 b_{W_i^*}^2 + \frac{3}{2} b_{\epsilon_{ei}}^2 \|B_i\|^2 + \frac{3}{2} \|B_i\|^2 b_{\Phi_{ei}} b_{\epsilon_{ei}} b_{W_i^*} + 12\beta^2$. Let the parameters be chosen such that $\mathcal{B}_i > 0$. Since \mathcal{A}_i is positive definite, the above Lyapunov derivative (63) is negative if

$$\left\| \tilde{W}_i \right\| > \frac{\mathcal{C}_i}{2\mathcal{B}_i} + \sqrt{\frac{\mathcal{C}_i^2}{4\mathcal{B}_i^2} + \frac{\mathcal{D}_i}{\mathcal{B}_i}}. \quad (64)$$

Thus, the weight learning error of the critic agent converges to the residual set

$$\tilde{\Omega}_{\tilde{W}_i} = \left\{ \tilde{W}_i \mid \left\| \tilde{W}_i \right\| \leq \frac{\mathcal{C}_i}{2\mathcal{B}_i} + \sqrt{\frac{\mathcal{C}_i^2}{4\mathcal{B}_i^2} + \frac{\mathcal{D}_i}{\mathcal{B}_i}} \right\}. \quad (65)$$

This completes the proof. \square

B The decoupled incremental subsystems of the 6-DoF quadrotor

This section presents the detailed procedures to decouple the 6-DoF quadrotor into 6 incremental subsystems.

Let $\zeta = [x, y, z]^\top \in \mathbb{R}^3$, and $\eta = [\phi, \theta, \psi]^\top \in \mathbb{R}^3$ represent the absolute linear position and Euler angles defined in the inertial frame, respectively. The E-L equation of a quadrotor follows (see [27])

$$m\ddot{\zeta} + mgI_z = RT_B \quad (66a)$$

$$J(\eta)\ddot{\eta} + C(\eta, \dot{\eta})\dot{\eta} = \tau_B, \quad (66b)$$

where $m \in \mathbb{R}^+$ denotes the mass of the quadrotor; $g \in \mathbb{R}^+$ is the gravity constant; $I_z = [0, 0, 1]^\top$ represents a column vector; $T_B = [0, 0, T]^\top \in \mathbb{R}^3$, where $T \in \mathbb{R}$ is the thrust in the direction of the body z -axis; $\tau_B = [\tau_\phi, \tau_\theta, \tau_\psi]^\top \in \mathbb{R}^3$ denotes the torques in the direction of the corresponding body frame angles; $R, J(\eta), C(\eta, \dot{\eta}) \in \mathbb{R}^{3 \times 3}$ represent the rotation matrix, Jacobian matrix, and Coriolis term, respectively. Their explicit forms are referred to [27].

Expanding the translational dynamics (66a) yields

$$\begin{aligned} \ddot{x} &= \frac{1}{m}T(C_\psi S_\theta C_\phi + S_\psi S_\phi) \\ \ddot{y} &= \frac{1}{m}T(S_\psi S_\theta C_\phi - C_\psi S_\phi) \\ \ddot{z} &= -g + \frac{1}{m}TC_\theta C_\phi \end{aligned} \quad (67)$$

where $C(\cdot)$ and $S(\cdot)$ denote $\cos(\cdot)$ and $\sin(\cdot)$, respectively.

By introducing pseudo controls $u_1 = T(C_\psi S_\theta C_\phi + S_\psi S_\phi)$, $u_2 = T(S_\psi S_\theta C_\phi - C_\psi S_\phi)$, and $u_3 = TC_\theta C_\phi$, and denoting $x_{11} = x$, $x_{12} = \dot{x}$, $x_{21} = y$, $x_{22} = \dot{y}$, $x_{31} = z$, $x_{32} = \dot{z}$, we finally decouple the transnational dynamics (66a) into the following three subsystems

$$\dot{x}_{11} = x_{12}, \quad \dot{x}_{12} = \frac{1}{m}u_1 \quad (68a)$$

$$\dot{x}_{21} = x_{22}, \quad \dot{x}_{22} = \frac{1}{m}u_2 \quad (68b)$$

$$\dot{x}_{31} = x_{32}, \quad \dot{x}_{32} = -g + \frac{1}{m}u_3. \quad (68c)$$

By following the same procedures clarified in Section 3, we get three subsystems for the rotational dynamics (66b):

$$\dot{x}_{41} = x_{42}, \quad \dot{x}_{42} = -\frac{H_1}{J_{11}} + \frac{1}{J_{11}}u_4 \quad (69a)$$

$$\dot{x}_{51} = x_{52}, \quad \dot{x}_{52} = -\frac{H_2}{J_{22}} + \frac{1}{J_{22}}u_5 \quad (69b)$$

$$\dot{x}_{61} = x_{62}, \quad \dot{x}_{62} = -\frac{H_3}{J_{33}} + \frac{1}{J_{33}}u_6, \quad (69c)$$

where $H_i = \sum_{j=1, j \neq i}^3 J_{ij}\ddot{\eta}_j + C_i\dot{\eta}_j \in \mathbb{R}$, $i = 1, 2, 3$; $u_4 = \tau_\phi$, $u_5 = \tau_\theta$, and $u_6 = \tau_\psi$.

The aforementioned procedures (67)-(69) allow us to get 6 subsystems in the same form as (3). Then, we could adopt our developed IADP based tracking control strategy, as clarified in Section 4, to drive the quadrotor (66) to track the predefined reference trajectory $x_r = [x_d, y_d, z_d, \psi_d]^\top$. Note that after the explicit values of pseudo controls u_1, u_2 , and u_3 are gotten, the trust T , and reference angles ϕ_d, θ_d are obtained as

$$T = \sqrt{u_1^2 + u_2^2 + u_3^2} \quad (70)$$

$$\phi_d = \arctan\left(\frac{u_1 S_\psi - u_2 C_\psi}{\sqrt{(u_1 C_\psi + u_2 S_\psi)^2 + u_3^2}}\right), \quad \phi_d \in \left(-\frac{\pi}{2}, \frac{\pi}{2}\right) \quad (71)$$

$$\theta_d = \arctan\left(\frac{u_1 C_\psi + u_2 S_\psi}{u_3}\right), \quad \theta_d \in \left(-\frac{\pi}{2}, \frac{\pi}{2}\right) \quad (72)$$

C The guidelines on hyperparameter selection

This section aims to offer guidelines to choose the values of k_{i_1} and k_{i_2} used in Δu_{i_f} (10). To offer hyperparameter tuning guidelines, we start by choosing a candidate Lyapunov function of the incremental error subsystem (12) as

$$V_i = \frac{1}{2}e_{i_1}^\top e_{i_1} + \frac{1}{2}e_{i_2}^\top e_{i_2}. \quad (73)$$

Calculating the derivative of (73) with regard to (12) and combining with (11), we get

$$\begin{aligned} \dot{V}_i &= e_{i_1}^\top e_{i_2} + e_{i_2}(-k_{i_1}e_{i_1} - k_{i_2}e_{i_2} + \bar{g}_i\Delta u_{i_b} + \bar{g}_i\xi_i) \\ &= (1 - k_{i_1})e_{i_1}^\top e_{i_2} - k_{i_2}e_{i_2}^\top e_{i_2} + e_{i_2}\varepsilon_i, \end{aligned} \quad (74)$$

where $\varepsilon_i = \bar{g}_i(\Delta u_{i_b} + \xi_i)$. According to (19), $\|\Delta u_{i_b}\| \leq \beta$ holds. Besides, $\|\xi_i\| \leq \bar{\xi}_i$ as proved in Lemma 1. Thus, it is concluded that $\|\varepsilon_i\| \leq \bar{g}_i(\beta + \bar{\xi}_i) := \bar{\varepsilon}_i$. Furthermore, the following equations hold

$$\begin{aligned} e_{i_1}^\top e_{i_2} &\leq \frac{1}{2}e_{i_1}^\top e_{i_1} + \frac{1}{2}e_{i_2}^\top e_{i_2} \\ e_{i_2}\varepsilon_i &\leq \frac{1}{2}e_{i_2}^\top e_{i_2} + \frac{1}{2}\varepsilon_i^\top \varepsilon_i \leq \frac{1}{2}e_{i_2}^\top e_{i_2} + \frac{1}{2}\bar{\varepsilon}_i^2. \end{aligned} \quad (75)$$

Then, substituting (75) into (74) yields

$$\dot{V}_i \leq \frac{1}{2}(1 - k_{i_1})e_{i_1}^\top e_{i_1} + (1 - k_{i_2} - \frac{k_{i_1}}{2})e_{i_2}^\top e_{i_2} + \frac{1}{2}\bar{\varepsilon}_i^2. \quad (76)$$

Thus, we could choose $k_{i_1} > 1$, and $k_{i_2} > \frac{1}{2}$ to meet $\dot{V}_i < 0$.